Letter

Experimental determination of a multiqubit ground state via a cluster mean-field algorithm

Ze Zhan,[1,*] Ying Fei,[1,*] Chongxin Run,[1,*] Zhiwen Zong,[1] Liang Xiang,[1] Wenyan Jin,[1] Zhilong Jia,[2] Peng Duan,[2] Guoping Guo,[2,3,†] Jianlan Wu,[1,‡] and Yi Yin[1,§]

[1]*Zhejiang Province Key Laboratory of Quantum Technology and Device, Department of Physics, Zhejiang University, Hangzhou 310027, China*

[2]*Key Laboratory of Quantum Information, University of Science and Technology of China, Hefei 230026, China*

[3]*Origin Quantum Computing, Hefei 230026, China*

(Received 30 August 2021; revised 10 September 2022; accepted 13 November 2022; published 8 December 2022)

A quantum eigensolver is designed under a multilayer cluster mean-field (CMF) algorithm by partitioning a quantum system into spatially-separated clusters. For each cluster, a reduced Hamiltonian is obtained after a partial average over its environment cluster. The products of eigenstates from different clusters construct a compressed Hilbert space, in which an effective Hamiltonian is diagonalized to determine certain eigenstates of the whole Hamiltonian. The CMF method is numerically verified in multispin chains and experimentally studied in a fully-connected three-spin network, both yielding an excellent prediction of their ground states.

DOI: 10.1103/PhysRevResearch.4.L042043

Introduction. At the dawn of a quantum computing era, applications on quantum simulation and beyond have attracted much attention of the whole quantum community. For example, mixed quantum-classical algorithms have been proposed in the goal of solving unaffordable quantum chemistry problems with quantum computers [1–9]. A variational quantum eigensolver (VQE) was successfully implemented in the determination of electronic states for a hydrogen molecule and multiatom hydrogen chains [1–4]. The adiabaticity and shortcut-to-adiabaticity (STA) in analog and digitized designs [5–8] can also be used in the quantum eigensolver, where an eigenstate of the target Hamiltonian is obtained by dragging an eigenstate of an initial Hamiltonian through an adiabatic or STA trajectory. Recently, we proposed a "leap-frog" algorithm via the digitized STA and adiabaticity [9]. Through a segmented trajectory of traveling intermediate states, our leap-frog method allows an efficient and reliable quantum eigensolver.

In the architecture of quantum computing, the eigenstructure of a 2^N-dimensional (2^N-D) Hilbert space can be determined in an N-qubit quantum device. However, the number of quantum gates in a digital quantum algorithm quickly increases with the number of qubits [10,11]. In addition, a multiqubit quantum gate is realized through a combination of single- and two-qubit gates [12] but the number of the combining gates increases with the gate size. The cost of quantum computing increases in company with the decrease of the fidelity so that a practical quantum eigensolver is still limited by the system size.

To improve this problem, some techniques have been developed, such as simplifying the specific target system [13], optimizing a particular algorithm of diagonalization [14]. A more general approach is to apply the idea from the classical field to reduce the computational dimension, such as the Krylov method [15–17], the divide-and-conquer method [18], and cluster-based methods. In the fields of physics and chemistry, cluster-based methods have been applied on various problems [19–22]. The concept of block spins was proposed to understand critical phenomena of the Ising model [19]. The clustering methods are also utilized in the quantum chemistry computation [20–22]. In the density matrix renormalization group (DMRG), the compression of the Hilbert space is realized by the diagonalization of reduced density matrices [20,21].

In this paper, we apply a multilayer cluster mean-field (CMF) theory [22] to build a new quantum eigensolver, from which the eigenstructure of a large-scale system can be reliably and efficiently determined in a much smaller-scale quantum device. The product states combined from the eigenstates of reduced cluster Hamiltonians define a compressed Hilbert space, in which the effective Hamiltonian is diagonalized for the eigensolver. This CMF method is numerically verified in N-spin chains and experimentally implemented in a fully-connected three-spin system, both yielding high fidelities for the extracted ground states.

Theory. In a general multi-electron system, the second quantized Hamiltonian can be transformed into a multi-spin form,

$$H = g^{(0)} + \sum_{i=1}^{N}\sum_{a=1}^{3} g^{(1)}_{i;a}\sigma_i^a + \sum_{i,j=1}^{N}\sum_{a,b=1}^{3} g^{(2)}_{ij;ab}\sigma_i^a\sigma_j^b + \sum_{i,j,k=1}^{N}\sum_{a,b,c=1}^{3} g^{(3)}_{ijk;abc}\sigma_i^a\sigma_j^b\sigma_k^c + \cdots, \quad (1)$$

*These authors have contributed equally to this work.
†gpguo@ustc.edu.cn
‡jianlanwu@zju.edu.cn
§yiyin@zju.edu.cn

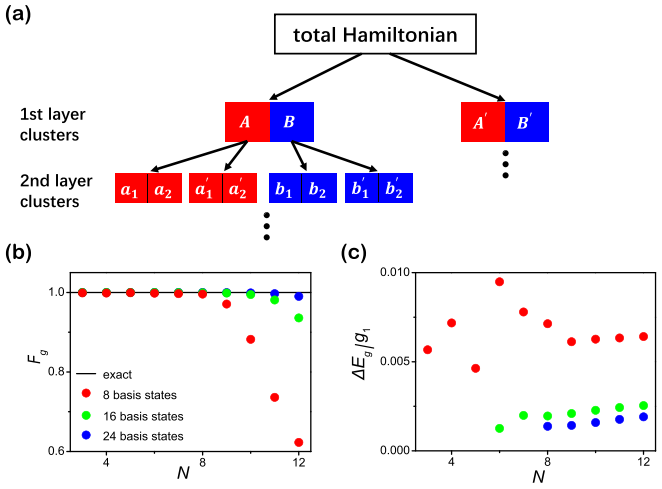

FIG. 1. (a) A schematic diagram of a multilayer CMF algorithm. (b), (c) The numerical calculation of this CMF method for the N-spin systems [the Hamiltonian in Eq. (3)]: (b) the fidelity $\mathcal{F}_g^{\text{theo}}$ of the ground state and (c) the energy difference $\Delta E_g = |E_g^{\text{theo}} - E_g^{\text{exact}}|$ between calculation and exact results. The red, green, and blue circles denote the numerical results of the CMF with 8, 16, and 24 product states applied to construct a compressed Hilbert space while the solid lines denote the exact results.

through a fermion-to-spin mapping method such as the Bravyi-Kitaev transformation [23]. Here $\{\sigma_i^a = X_i, Y_i, Z_i\}$ is the set of the Pauli matrices acting on spin i and the coefficients $\{g^{(0)}, g^{(1)}, g^{(2)}, \ldots\}$ describe the strengths of (multi)spin interactions. To keep its generality, Eq. (1) is allowed to include an arbitrary $N'(\leqslant N)$-spin interaction.

To extract the exact eigenstates and eigenenergies ($|\Psi_n\rangle$ and E_n) of the Hamiltonian in Eq. (1), we require a diagonalization tool in a 2^N-D Hilbert space. Instead, a CMF method can realize an approximate but reliable eigensolver in a highly compressed space. For simplicity, we assume that an N-spin network is divided into two clusters, each with N_A and $N_B(=N-N_A)$ spins. For a given N_A, the total choices of cluster partitioning are $M_{\max} = C_{N_A}^N$ but a practical number M can be much smaller than $M_{\max}$.

We interpret our CMF method as follows [see Fig. 1(a)]. For a given A-B partition, we inspect the two clusters separately. For cluster A, the rest part of the spin network (cluster B) is viewed as its environment. After a partial trace over a specific B-state $|\varphi_B^\alpha\rangle$, a reduced Hamiltonian $H_A^\alpha = \langle\varphi_B^\alpha|H|\varphi_B^\alpha\rangle$ is constructed and its diagonalization leads to a set of eigenstates $\{|\varphi_A^{i_\alpha}\rangle\}$ and eigenenergies $\{\varepsilon_A^{i_\alpha}\}$, i.e., $H_A^\alpha = \sum_i \varepsilon_A^{i_\alpha}|\varphi_A^{i_\alpha}\rangle\langle\varphi_A^{i_\alpha}|$. The same approach can be applied vice versa. With respect to an A-state $|\varphi_A^\beta\rangle$, the reduced B-Hamiltonian $H_B^\beta = \langle\varphi_A^\beta|H|\varphi_A^\beta\rangle$ is diagonalized into $H_B^\beta = \sum_j \varepsilon_B^{j_\beta}|\varphi_B^{j_\beta}\rangle\langle\varphi_B^{j_\beta}|$. The two sets of product states, $\{|\varphi_A^{i_\alpha}\rangle \otimes |\varphi_B^\alpha\rangle\}$ and $\{|\varphi_A^\beta\rangle \otimes |\varphi_B^{j_\beta}\rangle\}$, from all the necessary cluster partitions are mixed together to form a basis set of $\{|\psi_\gamma\rangle\}$ for a compressed Hilbert space. To capture a mean-field spirit, we expect that all the states are self-consistently determined, i.e., $\{|\varphi_A^{i_\alpha}\rangle\} = \{|\varphi_A^\beta\rangle\}$ and $\{|\varphi_B^{j_\beta}\rangle\} = \{|\varphi_B^\alpha\rangle\}$. Although the recursive iteration with both the ground and excited states included leads to more and more states, a limited number of relevant states are empirically selected. At the final step, irrelevant states are discarded and the Schmidt orthogonalization [24] is used to extract an orthonormal basis set $\{|\psi_\gamma^{\text{S}}\rangle\}$. An effective Hamiltonian,

$$H_{\text{eff}} = \sum_{\gamma\gamma'} H_{\gamma\gamma'}|\psi_\gamma^{\text{S}}\rangle\langle\psi_{\gamma'}^{\text{S}}| \tag{2}$$

with $H_{\gamma\gamma'} = \langle\psi_\gamma^{\text{S}}|H|\psi_{\gamma'}^{\text{S}}\rangle$, is thus defined. The digonalization of H_{eff} provides a good estimation of certain eigenstates $|\Psi_n\rangle$ and eigenenergies E_n. If the number of the product states associated with each cluster partition is J, the dimensionality of the compressed space is MJ, which can be significantly smaller than 2^N. The partition can be subsequently applied to clusters A and B, e.g., $A = a_1 \oplus a_2 = a_1' \oplus a_2' = \cdots$, which eventually leads to a multilayer CMF algorithm [see Fig. 1(a)]. Relatively speaking, our CMF method takes a top-down strategy by flexibly partitioning a large system into small clusters based on mean-field effect while the DMRG takes a bottom-up strategy by extending the system size with the increment of boundary spins.

Numerical study. To demonstrate the applicability of this CMF method, we numerically calculate the ground state $|\Psi_g\rangle$ and its eigenenergy E_g of an N-spin chain whose Hamiltonian reads [4]

$$H = \sum_{i=1}^{N} g_1 Z_i + \sum_{i=1}^{N-1} g_2 X_i X_{i+1}. \tag{3}$$

In our numerical calculation, the chain length is set to be $3 \leqslant N \leqslant 12$ while the two parameters are fixed at $g_2/g_1 = 2$. For each N-spin chain, we consider several choices of cluster partitioning, $\{A = \{s_1, s_2\}, B = \{s_3, \cdots s_N\}\}$, $\{A' = \{s_1, s_2, s_3\}, B' = \{s_4, \cdots s_N\}\}$, and $\{A'' = \{s_1, s_2, s_3, s_4\}, B'' = \{s_5, \cdots s_N\}\}\cdots$, where s_i denotes the ith spin. Taking the first cluster partition as an example, we show the numerical approach in detail. In the first stage, an initial B-state, $|\varphi_B\rangle \propto \prod_{n=3}^N (|+\rangle + |-\rangle)_n$, is used to obtain a reduced A-Hamiltonian,

$$H_A = \bar{\varepsilon}_A + g_1 Z_1 + g_1 Z_2 + g_1^A X_2 + g_2 X_1 X_2 \tag{4}$$

with $\bar{\varepsilon}_A = \sum_{n=3}^N g_1\langle\varphi_B|Z_n|\varphi_B\rangle + \sum_{n=3}^{N-1} g_2\langle\varphi_B|X_n X_{n+1}|\varphi_B\rangle$ and $g_1^A = g_2\langle\varphi_B|X_3|\varphi_B\rangle$. Due to the final goal of calculating $|\Psi_g\rangle$, we only select two A-eigenstates, the ground and first excited states of H_A, i.e., $\{|\varphi_A^\beta\rangle = |\varphi_A^g\rangle, |\varphi_A^e\rangle\}$. In the second stage, two B-Hamiltonians,

$$H_B^{\beta=g,e} = \bar{\varepsilon}_B + g_1^B X_3 + \sum_{n=3}^{N} g_1 Z_n + \sum_{n=3}^{N-1} g_2 X_n X_{n+1}, \tag{5}$$

are extracted with respect to these two A-eigenstates. The two parameters are given by $\bar{\varepsilon}_B = g_1\langle\varphi_A^\beta|Z_1 + Z_2|\varphi_A^\beta\rangle + g_2\langle\varphi_A^\beta|X_1 X_2|\varphi_A^\beta\rangle$ and $g_1^B = g_2\langle\varphi_A^\beta|X_2|\varphi_A^\beta\rangle$. The diagonalization of $H_B^{\beta=g,e}$ leads to four (ground and first excited) B-eigenstates, $|\varphi_B^{j_\beta}\rangle$ with $j = \{g, e\}$. In the third stage, we use these four B-states $|\varphi_B^\alpha\rangle$ ($\alpha = g_g, g_e, e_g, e_e$) as the environment states and calculate eight A-eigenstates $|\varphi_A^{i_\alpha}\rangle$ ($i = g, e$). To avoid the growing number of states, we stop at this stage and discard four crossing terms. The four remaining products are $|\varphi_A^{i_\alpha}\rangle \otimes |\varphi_B^\alpha\rangle$ with $\{i = g, \alpha = g_g, g_e\}$ and $\{i = e, \alpha = e_g, e_e\}$.

After including the relevant product states from the other cluster partitions, the Schmidt orthogonalization is applied to construct a compressed Hilbert space. The ground state $|\Psi_g\rangle$ and its eigenenergy E_g are then determined by the diagonalization of $H_{\rm eff}$ in Eq. (2).

In the case of $N(>4)$-spin chains, the two-layer approach is utilized. When one, two, or three types of cluster partitions are chosen, related basis states are the 8, 16, or 24 product states. We give a detailed cluster partition and complex analysis in the Supplemental Material [25]. The numerical results are presented in Figs. 1(b) and 1(c). We introduce a fidelity function, $\mathcal{F}_g^{\rm theo} = |\langle\Psi_g^{\rm exact}|\Psi_g^{\rm theo}\rangle|^2$. As shown in Fig. 1(b), the CMF predictions are excellent, satisfying $\mathcal{F}_g^{\rm theo}(3 \leqslant N \leqslant 8, 8\ \text{basis}) > 99.4\%$. When the total number of spins increases, the state fidelities in an 8-D Hilbert space would decrease. However, we can select more product states as basis states of the compressed Hilbert space to obtain high-fidelity results ($\mathcal{F}_g^{\rm theo}(8 \leqslant N \leqslant 12, 24\ \text{basis}) > 99.0\%$). As shown in Fig. 1(c), the accuracy of the ground state energy E_g is even higher ($\Delta E_g(3 \leqslant N \leqslant 12) < 0.01$).

Experimental study. Next we use a two-qubit device to extract $|\Psi_g\rangle$ and E_g of a fully-connected three-spin system as an experimental demonstration of the CMF algorithm. Due to the restriction of our current setup, it is difficult for us to reliably explore larger systems which will be left in the future. Our quantum device is composed of two superconducting cross-shaped transmon qubits [26–28]. The ground and excited states of each qubit are one-to-one mapped onto the spin up and down states, i.e., $|0\rangle \leftrightarrow |+\rangle$ and $|1\rangle \leftrightarrow |-\rangle$. The operation points of the two qubits are $\omega_a/2\pi = 5.46$ GHz and $\omega_b/2\pi = 4.92$ GHz, while their anharmonicities are $\Delta_a/2\pi \approx \Delta_b/2\pi = -250$ MHz. The relaxation times are $T_{a;1} = 16.1$ μs and $T_{b;1} = 26.5$ μs, and the pure dephasing times are $T_{a;\phi} = 20$ μs and $T_{b;\phi} = 45$ μs. The readout fidelities of the ground and excited states are $\{F_{a;0} = 99\%, F_{a;1} = 93\%\}$ and $\{F_{b;0} = 96\%, F_{b;1} = 94\%\}$.

The Hamiltonian of the three-spin system being studied is

$$H = g_1(Z_1 + Z_2 + Z_3) + g_2(X_1X_2 + X_2X_3) + g_3X_1X_2X_3, \tag{6}$$

where the three-spin interaction $X_1X_2X_3$ increases the difficulty of the eigensolver. In this Letter, two sets of experiments are performed to explore the influences of g_2/g_1 and g_3/g_1 separately. To visualize our experimental procedure, we take $g_2/g_1 = 1.0, g_3/g_1 = 0.1$ as an example and provide the stage-by-stage results in Fig. 2. (i) We treat spins one and two as cluster A and spin three as cluster B. With an initial guess of the B-state, $|\varphi_B\rangle = |1\rangle$, a reduced A-Hamiltonian is obtained as $H_A = H_A^0 + g_1^A X_2 + g_2^A X_1X_2$ with $H_A^0 = \bar{\varepsilon}_A + g_1Z_1 + g_1Z_2$. Here the B-averaged parameters are $\bar{\varepsilon}_A = g_1\langle\varphi_B|Z_3|\varphi_B\rangle$, $g_1^A = g_2\langle\varphi_B|X_3|\varphi_B\rangle$ and $g_2^A = g_2 + g_3\langle\varphi_B|X_3|\varphi_B\rangle$. The ground state of H_A is experimentally determined by a leap-frog algorithm via the digitized STA and adiabaticity [25]. With two varying parameters λ_1 and λ_2, the A-Hamiltonian is extended to be

$$H_A(\lambda_1, \lambda_2) = H_A^0 + \lambda_1 g_1^A X_2 + \lambda_2 g_2^A X_1X_2. \tag{7}$$

As shown in Fig. 2(a), we begin with an initial Hamiltonian $H_A^0 = H_A(\lambda_1 = 0, \lambda_2 = 0)$ and prepare its ground state $|\varphi_A^g(H_A^0)\rangle = |11\rangle$. A four-step digitized STA is applied to drag this state to the ground state $|\varphi_A^g(H_A^1)\rangle$ of an intermediate Hamiltonian $H_A^1 = H_A(\lambda_1 = 0, \lambda_2 = 0.1)$. Subsequently, two digitized adiabatic processes realize an evolution of $|\varphi_A^g(H_A^1)\rangle \to |\varphi_A^g(H_A(\lambda_1 = 0, \lambda_2 = 0.5))\rangle \to |\varphi_A^g(H_A)\rangle$. The theoretical prediction of the final state fidelity is $\mathcal{F}_g^{\rm theo} = 99.9\%$ while the experimental determination is at $\mathcal{F}_g^{\rm exp} = 98.6\%$. (ii) In the second stage [see Fig. 2(b)], we input the previous A-state $|\varphi_A^g\rangle$ and calculate the B-Hamiltonian, $H_B = H_B^0 + g_1^B X_3$ with $H_B^0 = \bar{\varepsilon}_B + g_1Z_3$. Here $\bar{\varepsilon}_B$ and g_1^B are two A-averaged parameters. The ground and excited states, $|\varphi_B^g(H_B)\rangle$ and $|\varphi_B^e(H_B)\rangle$, are experimentally determined via the digitized STA from the two initial states $|\varphi_B^g(H_B^0)\rangle = |1\rangle$ and $|\varphi_B^e(H_B^0)\rangle = |0\rangle$. The experimental fidelities of these two B-eigenstates are $\mathcal{F}_g^{\rm exp} \approx 99\%$. (iii) In the third stage, the two B-states, $|\varphi_B^g\rangle$ and $|\varphi_B^e\rangle$, are used to obtain two A-Hamiltonians, $H_A^{\alpha=g,e} = \langle\varphi_B^\alpha|H|\varphi_B^\alpha\rangle$, which are extended to the same form $H_A(\lambda_1, \lambda_2)$ as in Eq. (7) but the B-averaged parameters are updated. As shown in Figs. 2(c) and 2(d), the leap-frog algorithm is also applied to experimentally determine the ground state $|\varphi_A^{g_g}\rangle$ of H_A^g and the first excited state $|\varphi_A^{e_e}\rangle$ of H_A^e. The experimental fidelities are $\mathcal{F}^{\rm exp} = 99.2\%$ and 96.4% while their theoretical predictions

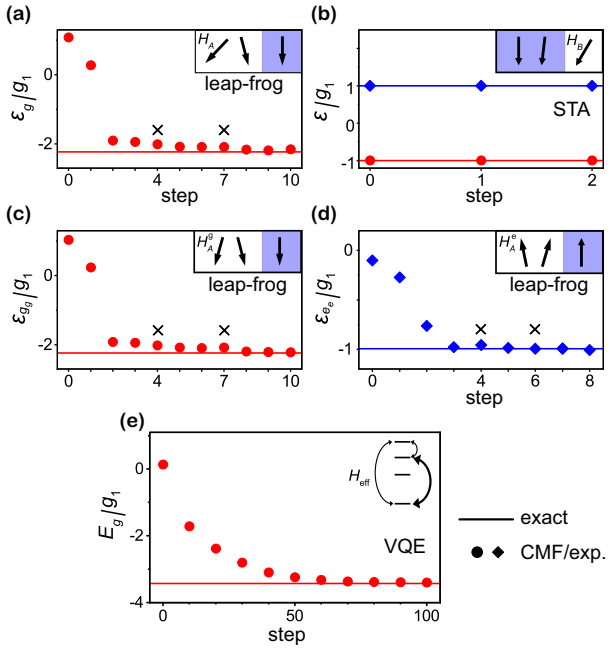

FIG. 2. A four-stage CMF experiment to determine the ground state $|\Psi_g\rangle$ for the three-spin Hamiltonian in Eq. (6) with $g_2/g_1 = 1.0$ and $g_3/g_1 = 0.1$. (a) The first-stage eigenenergy evolution in a three-segment leap-frog determination of $|\varphi_A^g\rangle$ for a reduced A-Hamiltonian H_A. (b) The second-stage eigenenergy evolutions in the digitized STA determination of $|\varphi_B^g\rangle$ and $|\varphi_B^e\rangle$ for the subsequent B-Hamiltonian H_B. (c), (d) The third-stage eigenenergy evolutions in the leap-frog determinations of (c) $|\varphi_A^{g_g}\rangle$ and (d) $|\varphi_A^{e_e}\rangle$ for H_A^g and H_A^e, respectively. The cluster partition is shown in the inset of each panel. In (a), (c), and (d), each cross labels a segment boundary in the three-segment leap-frog algorithm. (e) The fourth-stage eigenenergy evolution in the VQE determination of $|\Psi_g\rangle$ for the 4D effective Hamiltonian $H_{\rm eff}$. The inset shows the structure of $H_{\rm eff}$ (Eq. 2). In each panel, the symbols denote the experimental results and the solid horizontal lines label their exact values.

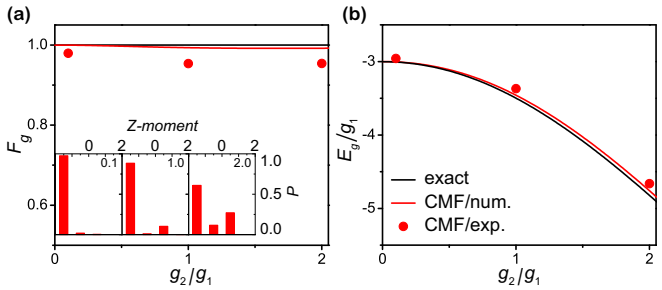

FIG. 3. The CMF determination of (a) the fidelity of the ground state $|\Psi_g\rangle$ and (b) the corresponding eigenenergy E_g for the three-spin Hamiltonian in Eq. (6) with a fixed $g_3/g_1 = 0.1$ and a varying g_2/g_1. The red lines and circles denote the numerical and experimental results via the CMF method while the black lines denote the exact values. In the inset of (a), the distributions of the Z moment are shown for the experimentally determined $|\Psi_g^{\rm exp}\rangle$ with $g_2/g_1 = 0.1$, 1.0, and 2.0.

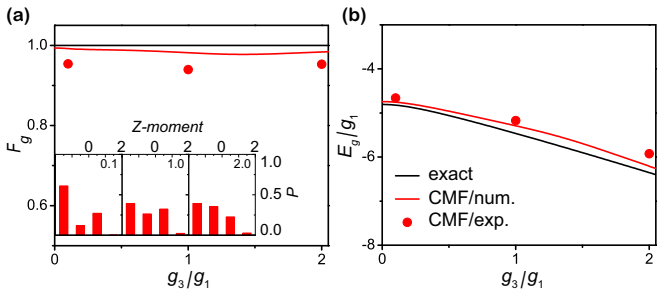

FIG. 4. The CMF determination of (a) the fidelity of the ground state $|\Psi_g\rangle$ and (b) the corresponding eigenenergy E_g for the three-spin Hamiltonian in Eq. (6) with a fixed $g_2/g_1 = 2.0$ and a varying g_3/g_1. The red lines and circles denote the numerical and experimental results via the CMF method while the black lines denote the exact values. In the inset of (a), the distributions of the Z moment are shown for the experimentally determined $|\Psi_g^{\rm exp}\rangle$ with $g_3/g_1 = 0.1$, 1.0, and 2.0.

are both $\mathcal{F}^{\rm theo} = 99.8\%$. (iv) The above iteration stages lead to two product states, $\{|\psi_{\gamma=1,2}\rangle = |\varphi_A^{g_g}\rangle \otimes |\varphi_B^{g}\rangle, |\varphi_A^{e_e}\rangle \otimes |\varphi_B^{e}\rangle\}$. Following a symmetry argument, the other two product states $\{|\psi_{\gamma=3,4}\rangle\}$ are obtained for the cluster partition of $A' = \{\text{spins } 2, 3\}$ and $B' = \{\text{spin } 1\}$. The subsequent Schmidt orthogonalization gives rise to four orthogonal basis states $\{\psi^{\rm S}_{\gamma=1,\ldots,4}\rangle\}$ and a 4-D effective Hamiltonian $H_{\rm eff}$. As shown in Fig. 2(e), the experimental determination of $|\Psi_g^{\rm exp}\rangle$ is converged over $70 \sim 100$ VQE steps, with a high fidelity $\mathcal{F}_g^{\rm exp} = 95.4\%$ as compared to the theoretical prediction $\mathcal{F}_g^{\rm theo} = 99.3\%$. All the experimental states are measured by quantum state tomography and then stored in the classical computer for following calculations. A detailed cluster error analysis is shown in the Supplemental Material [25].

In the first stage of our experiment, we only consider the ground state of H_A so that the total four product states arisen from its first excited state are excluded. The inset in Fig. 2(e) shows a schematic diagram of the effective Hamiltonian, from which we find that $|\Psi_g\rangle$ can be obtained from the 3D or 2D spaces with $\mathcal{F}_g^{\rm theo} = 99.3\%$ and 99.0%. Thus, a continued compression over the product states is allowed to further decrease the cost of a CMF eigensolver.

In Fig. 3, we present our first set of the experimental results of $|\Psi_g^{\rm exp}\rangle$ and $E_g^{\rm exp}$ for a fixed $g_3/g_1 = 0.1$ and a varying g_2/g_1 ($= 0.1$, 1.0, and 2.0) based on the CMF algorithm. As compared to the exact ground state, the theoretical predictions of the state fidelity is excellent ($\mathcal{F}_g^{\rm theo} > 99\%$) while the experimental results are consistently high, $\mathcal{F}_g^{\rm exp} =$ 97.9%, 95.4%, and 95.4% [see Fig. 3(a)]. The same behavior is found for the accuracy of $E_g^{\rm exp}$ [see Fig. 3(b)]. In a simplified scenario of $g_3 = 0$, this three-spin system prefers ferromagnetism along the Z direction for $g_2/g_1 \to 0$ while antiferromagnetism along the X direction in the opposite limit ($g_2/g_1 \to \infty$). The ground state thus experiences a transition from $|\Psi_g(g_2/g_1 \to 0)\rangle = |111\rangle$ to $|\Psi_g(g_2/g_1 \to \infty)\rangle \propto \prod_{i=1}^{3}(|0\rangle - (-1)^i|1\rangle)_i$. From the quantum statistics in many experiments, we measure the distribution of the total spin moment $M_j = \sum_{i=1}^{N} m_{i;j}$, where $m_{i;j}$ is the magnetic moment of each ith spin along the $j(= X, Y, Z)$ direction. In the parameter range in our experiment, the entanglement of $|\Psi_g\rangle$ increases with g_2/g_1, indicated by a broadening distribution of the Z moment M_Z in the inset of Fig. 3(a).

In our second set of experiments, we fix $g_2/g_1 = 2.0$ and consider three values of $g_3/g_1 = 0.1$, 1.0, and 2.0. As shown in the inset of Fig. 4(a), the increase of g_3/g_1 also leads to an extensive distribution of the Z moment. The same CMF algorithm as in Fig. 2 reliably determines the ground states. The experimental results of the state fidelities are presented in Fig. 4(a), satisfying $\mathcal{F}_g^{\rm exp} = 95.4\%$, 94.0%, and 95.3% for the three input parameters. The accuracy of the experimentally extracted eigenenergy $E_g^{\rm exp}$ follows the same trend [see Fig. 4(b)].

Summary. In this Letter, we apply a multilayer CMF method to design a new quantum eigensolver so that the eigenstates of a large-scale quantum system can be determined by a series of quantum computations over its clusters. For a preselected cluster, certain eigenstates of its reduced Hamiltonian are extracted via a quantum eigensolver (e.g., leap-frog, VQE) after a partial average over an eigenstate of the environment cluster. The products of eigenstates from different clusters are used to construct a compressed Hilbert space, in which the effective Hamiltonian is diagonalized to determine certain eigenstates of the whole Hamiltonian. This CMF method is numerically verified in the $N(3 \leqslant N \leqslant 12)$-spin chains with two-spin interactions and further experimentally studied in the three-spin chain with both two- and three-spin interactions. The determination of the ground states in compressed spaces provide an excellent prediction. The studies of the ground states in this paper can be straightforwardly extended to the excited states.

In addition to our CMF method, other ideas of compressing Hilbert space can also be applied to the quantum eigensolver, such as the divide-and-conquer method and Krylov method [15–18]. Their practical realization needs to be further verified experimentally. In principle, the divide-and-conquer method divides Hamiltonian directly and generates basis by excitation operations and the Krylov method generates nonorthogonal basis by Krylov subspace span. Our CMF method with an

intuitive physical picture might be more flexible in different applications.

With a size increment of quantum devices, the CMF method shows its theoretical promise to sufficiently large-scale Hilbert spaces [29]. We also believe that our CMF method deserves more thought when applied in a more extensive experimental implementation. For example, due to the difficulty of large-scale quantum state measurement in quantum device, measuring the elements of the effective Hamiltonian instead of quantum states [30,31] or optimizing quantum-state-tomography (e.g., shadow tomography [32] and the probably approximate correct learning [33]) might be further research directions in the future.

Acknowledgments. The work reported here was supported by the National Key Research and Development Program of China (Grants No. 2019YFA0308602 and No. 2016YFA0301700), the National Natural Science Foundation of China (Grants No. 12074336, No. 11934010, and No. 11775129), the Fundamental Research Funds for the Central Universities in China (2020XZZX002-01), and the Anhui Initiative in Quantum Information Technologies (Grant No. AHY080000). Y.Y. acknowledge the funding support from Tencent Corporation. This work was partially conducted at the University of Science and Technology of China Center for Micro- and Nanoscale Research and Fabrication.

[1] A. Peruzzo, J. McClean, P. Shadbolt, M. Yung, X. Zhou, P. J. Love, A. Aspuru-Guzik, and J. L. O'Brien, A variational eigenvalue solver on a photonic quantum processor, Nat. Commun. **5**, 4213 (2014).

[2] A. Kandala, A. Mezzacapo, K. Temme, M. Takita, M. Brink, J. M. Chow, and J. M. Gambetta, Hardware-efficient variational quantum eigensolver for small molecules and quantum magnets, Nature (London) **549**, 242 (2017).

[3] J. I. Colless, V. V. Ramasesh, D. Dahlen, M. S. Blok, M. E. Kimchi-Schwartz, J. R. McClean, J. Carter, W. A. de Jong, and I. Siddiqi, Computation of Molecular Spectra on a Quantum Processor with an Error-Resilient Algorithm, Phys. Rev. X **8**, 011021 (2018).

[4] Google AI Quantum and Collaboration, Hartree-Fock on a superconducting qubit quantum computer, Science **369**, 1084 (2020).

[5] E. Farhi, J. Goldstone, S. Gutmann, J. Lapan, A. Lundgren, and D. Preda, A quantum adiabatic evolution algorithm applied to random instances of an NP-complete problem, Science **292**, 472 (2001).

[6] R. Barends, A. Shabani, L. Lamata, J. Kelly, A. Mezzacapo, U. L. Heras, R. Babbush, A. G. Fowler, B. Campbell, Yu Chen *et al.*, Digitized adiabatic quantum computing with a superconducting circuit, Nature (London) **534**, 222 (2016).

[7] X. Chen, I. Lizuain, A. Ruschhaupt, D. Guéry-Odelin, and J. G. Muga, Shortcut to Adiabatic Passage in Two- and Three-Level Atoms, Phys. Rev. Lett. **105**, 123003 (2010).

[8] N. N. Hegade, K. Paul, Y. Ding, M. Sanz, F. Albarran-Arriagada, E. Solano, and X. Chen, Shortcuts to Adiabaticity in Digitized Adiabatic Quantum Computing, Phys. Rev. Appl. **15**, 024038 (2021).

[9] Z. Zhan, C. Run, Z. Zong, L. Xiang, Y. Fei, Z. Sun, Y. Wu, Z. Jia, P. Duan, J. Wu, Y. Yin, and G. Guo, Experimental Determination of Electronic States via Digitized Shortcut to Adiabaticity and Sequential Digitized Adiabaticity, Phys. Rev. Appl. **16**, 034050 (2021).

[10] S. Lloyd, Universal quantum simulators, Science **273**, 1073 (1996).

[11] R. Barends, L. Lamata, J. Kelly, L. García-Álvarez, A. G. Fowler, A. Megrant, E. Jeffrey, T. C. White, D. Sank, J. Y. Mutus *et al.*, Digital quantum simulation of fermionic models with a superconducting circuit, Nat. Commun. **6**, 7654 (2015).

[12] S. Lloyd, Almost Any Quantum Logic Gate is Universal, Phys. Rev. Lett. **75**, 346 (1995).

[13] K. Setia, R. Chen, J. E. Rice, A. Mezzacapo, M. Pistoia, and J. D. Whitfield, Reducing qubit requirements for quantum simulations using molecular point group symmetries, J. Chem. Theory Comput. **16**, 6091 (2020).

[14] J. S. Kottmann and A. Aspuru-Guzik, Optimized low-depth quantum circuits for molecular electronic structure using a separable-pair approximation, Phys. Rev. A **105**, 032449 (2022).

[15] W. J. Huggins, J. Lee, U. Baek, B. ÓGorman, and K. B. Whaley, A non-orthogonal variational quantum eigensolver, New J. Phys. **22**, 073009 (2020).

[16] K. Seki and S. Yunoki, Quantum power method by a superposition of time-evolved states, PRX Quantum **2**, 010333 (2021).

[17] C. L. Cortes and S. K. Gray, Quantum Krylov subspace algorithms for ground-and excited-state energy estimation, Phys. Rev. A **105**, 022417 (2022).

[18] K. Fujii, K. Mizuta, H. Ueda, K. Mitarai, W. Mizukami, and Y. O. Nakagawa, Deep Variational Quantum Eigensolver: a divide-and-conquer method for solving a larger problem with smaller size quantum computers, PRX Quantum **3**, 010346 (2022).

[19] L. P. Kadanoff, Scaling laws for Ising models near Tc, Phys. Phys. Fiz. **2**, 263 (1966).

[20] S. R. White, Density Matrix Formulation for Quantum Renormalization Groups, Phys. Rev. Lett. **69**, 2863 (1992).

[21] U. Schollwöck, The density-matrix renormalization group, Rev. Mod. Phys. **77**, 259 (2005).

[22] C. A. Jiménez-Hoyos and G. E. Scuseria, Cluster-based mean-field and perturbative description of strongly correlated fermion systems: Application to the one-and two-dimensional Hubbard model, Phys. Rev. B **92**, 085101 (2015).

[23] J. T. Seeley, M. J. Richard, and P. J. Love, The Bravyi-Kitaev transformation for quantum computation of electronic structure, J. Chem. Phys. **137**, 224109 (2012).

[24] Å. Björck, Solving linear least squares problems by Gram-Schmidt orthogonalization, BIT **7**, 1 (1967).

[25] See Supplemental Material at http://link.aps.org/supplemental/10.1103/PhysRevResearch.4.L042043 for the discussion of the leap-frog algorithm, complexity and error analysis.

[26] A. A. Houck, D. I. Schuster, J. M. Gambetta, J. A. Schreier, B. R. Johnson, J. M. Chow, L. Frunzio, J. Majer, M. H.

Devoret, S. M. Girvin, and R. J. Schoelkopf, Generating single microwave photons in a circuit, Nature (London) **449**, 328 (2007).

[27] R. Barends, J. Kelly, A. Megrant, D. Sank, E. Jeffrey, Y. Chen, Y. Yin, B. Chiaro, J. Mutus, C. Neill *et al.*, Coherent Josephson Qubit Suitable for Scalable Quantum Integrated Circuits, Phys. Rev. Lett. **111**, 080502 (2013).

[28] L. Xiang, Z. Zong, Z. Sun, Z. Zhan, Y. Fei, Z. Dong, C. Run, Z. Jia, P. Duan, J. Wu, Y. Yin, and G. Guo, Simultaneous Feedback and Feedforward Control and Its Application to Realize a Random Walk on the Bloch Sphere in an Xmon-Superconducting-Qubit System, Phys. Rev. Appl. **14**, 014099 (2020).

[29] F. Arute, K. Arya, R. Babbush, D. Bacon, J. C. Bardin, R. Barends, R. Biswas, S. Boixo, F. G. S. L. Brandao, D. A. Buell *et al.*, Quantum supremacy using a programmable superconducting processor, Nature (London) **574**, 505 (2019).

[30] H. Buhrman, R. Cleve, J. Watrous, and R. de Wolf, Quantum Fingerprinting, Phys. Rev. Lett. **87**, 167902 (2001).

[31] Y. Ibe, Y. O. Nakagawa, N. Earnest, T. Yamamoto, K. Mitarai, Q. Gao, and T. Kobayashi, Calculating transition amplitudes by variational quantum deflation, Phys. Rev. Res. **4**, 013173 (2022).

[32] S. Aaronson, In Proceedings of the 50th Annual ACM SIGACT Symposium on Theory of Computing, STOC **18**, 325 (2018).

[33] A. Rocchetto, S. Aaronson, S. Severini, G. Carvacho, D. Poderini, I. Agresti, M. Bentivegna, and F. Sciarrino, Experimental learning of quantum states, Sci. Adv. **5**, eaau1946 (2019).